**Computers and Concrete**, *Vol. 16, No. 4 (2015) 545-568*
DOI: http://dx.doi.org/10.12989/cac.2015.16.4.545 

# Increasing the flexural capacity of RC beams using partially HPFRCC layers

Ali Hemmati[*1], Ali Kheyroddin[2a] and Mohammad K. Sharbatdar[3b]

[1]*Department of Civil Engineering, Semnan Branch, Islamic Azad University, Semnan, Iran*
[2]*Civil Engineering Faculty, Semnan University, Iran and Visiting Scholar in Department of Civil Engineering and Applied Mechanics, University of Texas, Arlington, TX, USA*
[3]*Civil Engineering Faculty, Semnan University, Semnan, Iran*

*(Received April 9, 2011, Revised October 19, 2015, Accepted October 22, 2015)*

**Abstract.** High Performance Fiber Reinforced Cementitious Composites which are called HPFRCC, include cement matrices with strain hardening response under tension loading. In these composites, the cement mortar with fine aggregates, is reinforced by continuous or random distributed fibers and could be used for various applications including structural fuses and retrofitting of reinforced concrete members etc. In this paper, mechanical properties of HPFRCC materials are reviewed briefly. Moreover, a reinforced concrete beam (experimentally tested by Maalej *et al.*) is chosen and in different specimens, lower or upper or both parts of that beam are replaced with HPFRCC layers. After modeling of specimens in ABAQUS and calibration of those, mechanical properties of these specimens are investigated with different thicknesses, tensile strengths, tensile strains and compressive bars. Analytical results which are obtained by nonlinear finite analyses show that using HPFRCC layers with different parameters, increase loading capacity and ultimate displacement of these beams compare to RC specimens.

**Keywords:** beam; HPFRCC; nonlinear finite element; reinforced concrete; ultimate load; ultimate displacement

## 1. Introduction

Strength, stiffness, toughness (the area under the stress-strain curve) and durability are the main characteristics of a High Performance Material (Brandt 2008). At first steps, Li and Wu introduced a pseudo-strain-hardening material that uses only fine aggregates with reinforcing polyethylene fibers (Li and Wu 1992). In 1996, Naaman and Reinhardt presented and developed a fiber reinforced cementitious material which had a matrix with no coarse aggregates, and regarded as fiber reinforced cement paste or mortar (Naaman and Reinhardt 1996). As it shown in Fig. 1, high tensile ductility with strain hardening response is the most important characteristics of this material which is called as High Performance Fiber Reinforced Cementitious Composite (HPFRCC). In

*Corresponding author, Assistant Professor, E-mail: a.hemmati@semnaniau.ac.ir
[a]Professor
[b]Associate Professor


http://www.techno-press.org/?journal=cac&subpage=8 ISSN: 1598-8198 (Print), 1598-818X (Online)

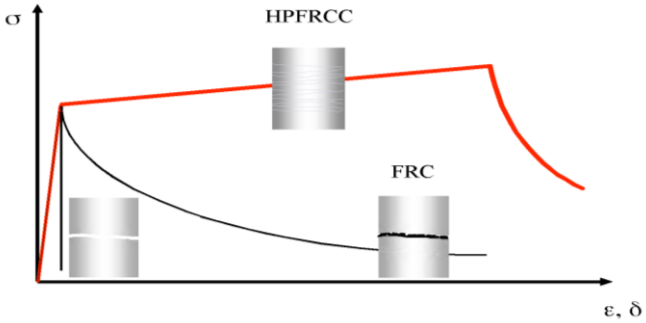


Fig. 1 Tensile stress-strain curves of concrete, FRC and HPFRCC (Fischer and Li 2000)

Table 1 Major physical properties of ECC (Li 2007)

| Compressive Strength (MPa) | First Cracking Strength (MPa) | Ultimate Tensile Strength (MPa) | Ultimate Tensile Strain (%) | Young's Modulus (GPa) | Flexural Strength (MPa) | Density (gr/cc) |
|---|---|---|---|---|---|---|
| 20-95 | 3-7 | 4-12 | 1-8 | 18-34 | 10-30 | 0.95-2.3 |

recent years, a new class of HPFRCC has emerged entitled ECC. Engineered Cementitious Composite (ECC) originally developed at the University of Michigan, with a typical moderate tensile strength of 4-6 MPa and a higher ductility of 3-5% (Fischer *et al.* 2003). After this stage, self-consolidating ECC, high early strength ECC, light weight ECC and green ECC were introduced by different researchers (Kong *et al.* 2003, Wang and Li 2006, Wang and Li 2003, Lepech *et al.* 2007). A summary of major physical properties of ECC is given in Table 1 (Li 2007).

A large number of researches which have been developed around ECC material based on PVA fiber. But, decision making on selecting the type of fibers to use, depends on fiber's natural characteristics such as diameter ranges, surface characteristics and mechanical behavior. It also depends on the matrix cracking properties, fiber-matrix interfacial bonding properties, the desired properties of the ECC composites, the durability needed, the desired sustainability of the system and the economic constraints of the application. (Lee *et al.* 2010).

Maalej and Li proposed a new design method for improving the durability of RC flexural members. In this method, a layer of ECC was substituted for the lower part of a reinforced concrete beam. Experimental results showed that, crack width could be controlled which may be improve durability. The geometry of this R.C. beam with ECC layer is shown in Fig. 2 (Maalej and Li 1995). Maalej *et al.* performed another experimental program on the influence of DFRCC (a type of HPFRCC with deflection hardening in flexure) in retarding the corrosion of steel in R.C. beams. Experimental results showed, when a layer of DFRCC material was used in lower segment of the beam, this composite beam had a noticeably higher resistance against steel corrosion compared to a regular R.C. beam (Maalej *et al.* 2002).

Some of the researchers have worked on nonlinear finite element analysis of concrete, composite and HPFRCC sections (Ghobarah and Aly 1998, Shaheen and Shrive 2008, Ranzi and Bradford 2009, Zhu *et al.* 2013). Results showed that there is an appropriate compatibility between experimental tests and analytical investigations in regard of HPFRCC (Han *et al.* 2003, Sirijaroonchai 2009, Mortezaei and Kheyroddin and Ronagh 2010, Na and Kwak 2011).

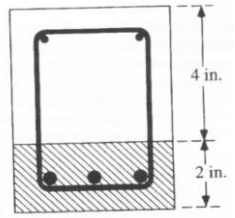


Fig. 2 Geometry of R.C. beam with ECC layer (Maalej and Li 1995)

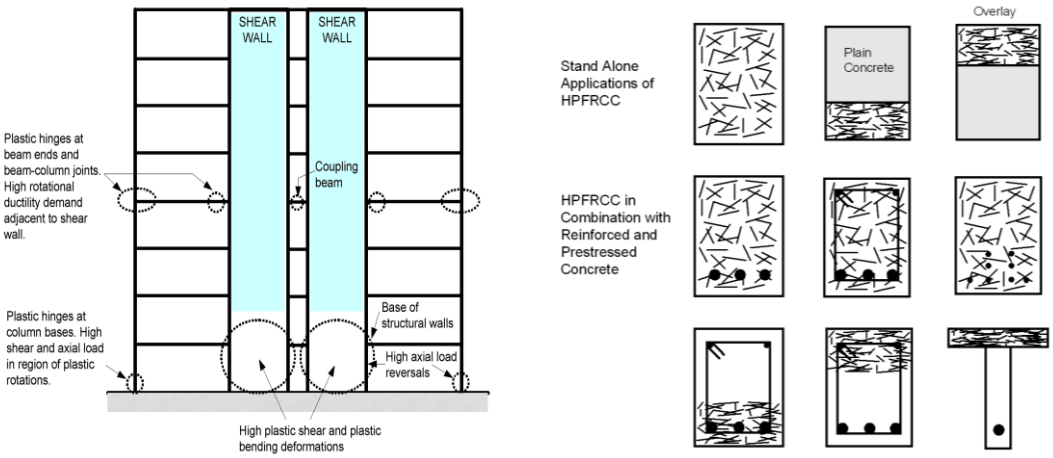


Fig. 3 Application of HPFRCC in structures and members (Shai and Mo 2008)

## 2. Tensile characteristics of ECC

As it mentioned earlier, the most important characteristic of ECC is the high tensile ductility with strain capacity as high as 1-8%. As it shown in Fig. 1, under the uni-axial tension loading of an ECC specimen and at the end of the elastic stage, the first micro-cracks appear. After this stage, both deformation and tension load increase with lower slope than the first stage which is called strain hardening. During this stage, multiple cracks form in different parts of the specimen and these cracks do not concentrated at a one plane. Hence, a rise in deformation and tension load occurs until a localized fracture plane (or a Griffith-type fracture plane) is formed. Beyond this peak load, ECC is no different than normal concrete or FRC, showing a tension-softening response.

The use of high performance materials such as HPFRCC, when considered as an alternative in design, is not necessary throughout the structure. In most cases, only a small part of the structure or a member may be constructed by these materials. Some examples include the beam-columns connections in earthquake resistant frames, the lower sections of shear walls or the lower columns in high rise buildings, link beam in coupled shear walls, damper system in buildings with soft story, frames with infill HPFRCC walls and other structural members which are shown in Fig. 3 (Shai and Mo 2008, Parsekian *et al.* 2008, Chao *et al.* 2008).

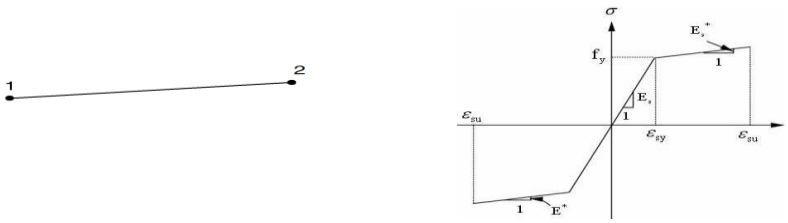


Fig. 4 Stress-strain curve and nonlinear element of reinforcing bars (ABAQUS 2008)

## 3. Research significance

A survey of literature shows that more analytical work is needed to investigate the use of HPFRCC material instead of normal concrete in beams and a research program must be established for investigating the structural behavior of a R.C. beam with HPFRCC layers. A great amount of researches which have been performed by Maalej and Li in recent years, focused on the durability and steel corrosion of these composite beams and it is necessary to evaluate the structural behavior of these hybrid members. Moreover, some numerical works have been performed by Kabele for numerically simulating of an ECC overlay cast on an un-reinforced concrete beam with a notched fracture (Kabele 2000). The depth of HPFRCC material which should be applied instead of the concrete in beams must be studied more to achieve the optimum option. This paper examines the complete nonlinear response of a R.C. single-bay beam tested under monotonically increasing loads using the nonlinear finite element approach. Moreover, the software is used to carry out a plastic analysis of the beam to define mechanism of failure, formation of cracks and ultimate displacements.

## 4. Nonlinear finite element program

ABAQUS is a powerful engineering simulation programs, based on the finite element method that can perform nonlinear analyses. In a nonlinear analysis, ABAQUS automatically chooses appropriate load increments and convergence tolerances and continually adjusts them during the analysis to ensure that an accurate solution is obtained efficiently (ABAQUS 2008). The reinforcing bars are modeled as an elastic strain hardening material as shown in Fig. 4 by a 2 node nonlinear truss element.

In this paper, concrete damage plasticity is selected for modeling of concrete and HPFRCC materials. The actual stress-strain curve of HPFRCC which is presented by various researchers and is very close to regular concrete, could be entered in damage plasticity model and calibrated with experimental work (Han *et al.* 2003, Hung and El-Tawil 2010, Gencturk and Elnashai 2012, Hemmati *et al.* 2014).The model is a continuum, plasticity-based, damage model for concrete. It assumes that the main two failure mechanisms are tensile cracking and compressive crushing of the concrete material. The evolution of the yield (or failure) surface is controlled by two hardening

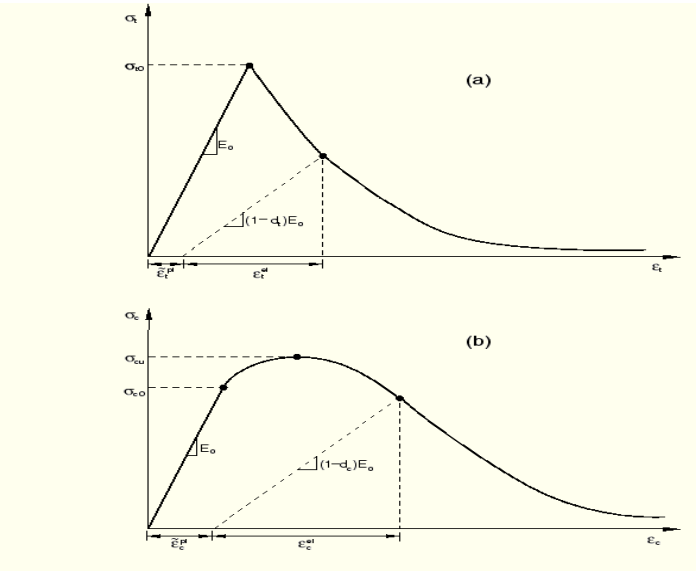


(a) tension and (b) com pression (ABAQUS 2008)

Fig. 5 Response of concrete

variables ($\tilde{\varepsilon}_t^{pl}$ and $\tilde{\varepsilon}_c^{pl}$) linked to failure mechanisms under tension and compression loading, respectively. The model assumes that the uni-axial tensile and compressive response of concrete is characterized by damaged plasticity, as shown in Fig. 6 (ABAQUS 2008). $\varepsilon_t$ and $\varepsilon_c$ are tensile and compressive strain respectively. Some researchers have been developed other plasticity based models for HPFRCC material too (Kabele and Horii 1996, Sirijaroonchai 2009).

If $E_0$ is the initial (undamaged) elastic stiffness of the material, the stress-strain relations under uni-axial tension and compression loading are introduced by Eq. (1)

$$\begin{aligned} \sigma_t &= (1-d_t)E_0\left(\varepsilon_t - \tilde{\varepsilon}_t^{pl}\right) \\ \sigma_c &= (1-d_c)E_0\left(\varepsilon_c - \tilde{\varepsilon}_c^{pl}\right) \end{aligned} \tag{1}$$

Where, $d_t$ and $d_c$ are two damage variables in tension and compression (0=undamaged material and 1=total loss of strength).

The concrete and HPFRCC are modeled as elastic strain softening and elastic strain hardening materials in tension as shown in Fig. 5 and Fig. 6 respectively. A 3-D nonlinear solid element with ability to modeling the composite sections is applied to model these beams (Fig. 7). The compression behavior of these two materials is the same (Fukuyama *et al.* 2000). As it shown in Fig. 6, $\sigma_{cc}$ and $\sigma_{pc}$ are the first cracking stress and the maximum stress of HPFRCC with PVA fibers in the range of 0.75%-2% and are expressed by Eq. (2) (Suwannakarn 2009)

$$\begin{aligned} \sigma_{cc} &= \sigma_{mu}\left(1-V_f\right) + 0.5204\tau V_f \, L/d \\ \sigma_{pc} &= (-0.7074V_f + 2.0933)\tau V_f \, L/d \end{aligned} \tag{2}$$

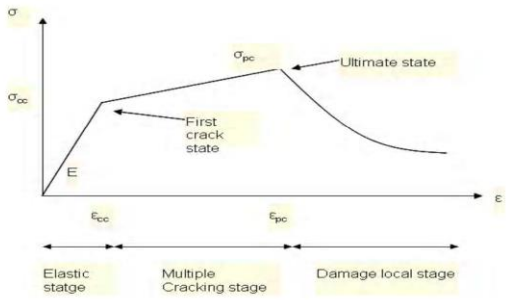


Fig. 6 Tensile behavior of HPFRCC (Fukuyama *et al.* 2000)

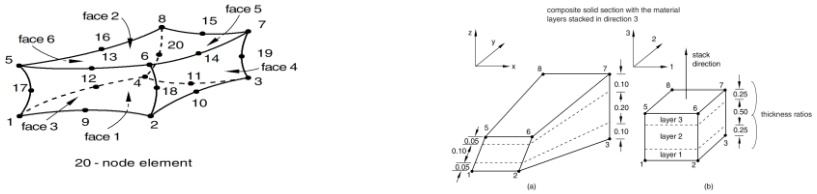


Fig. 7 Nonlinear element for modeling of concrete and HPFRCC (ABAQUS 2008)

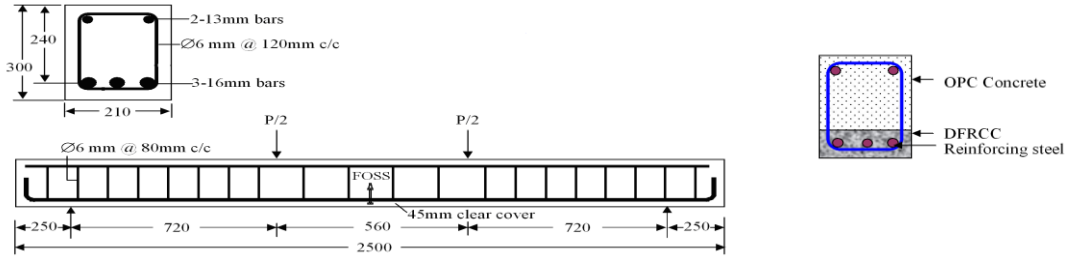


Fig. 8 Details of the experimental specimen (Maalej *et al.* 2002)

Where, $\sigma_{mu}$=Tensile strain of matrix, $V_f$=Volume fraction of fiber, $\tau$=Average bond strength at the fiber matrix interface, $L$=Fiber length and $d$=Fiber diameter.

## 5. Modeling and calibration with experimental work

An experimental investigation was undertaken to corroborate the analytical work and lend further insight into the nature of finite element items in beam. The test model which was chosen for this analytical study, was a large scale beam with two hinged supports, which has been tested by Maalej *et al.* (2002). The beam span is 2500 mm and the cross section of the beam is constant throughout at 300 mm deep by 210 mm wide. 2-point loading which is increased monotically applied on this beam. Details of reinforcement layout and loading of the beam are shown in Fig. 8. Material properties are summarized in Table 2.

In the experimental program, RC beam was cast under low frequency vibration in one step. In the composite beam, the ECC layer was first poured in the mold under low frequency vibration

Table 2 Concrete and steel properties used in the test beam

| Dimensions and properties of the materials | Maalej *et al.* (RC beam) (2002) | Maalej *et al.* (Composite beam) (2002) |
|---|---|---|
| $d$ (mm) | 240 | 240 |
| $A_S$ (mn$^2$) | 603 | 603 |
| $A'_S$ (mm$^2$) | 265.3 | 265.3 |
| $f'_c$ (MPa) Concrete | 41.6 | 41.6 |
| $f'_c$ (MPa) *HPFRCC* | - | 61.3 |
| $\varepsilon_{cu}^*$ | 0.004 | 0.004 |
| $f_y$ (MPa) | 415 | 415 |
| $E_S$ (MPa) | 200,000 | 200,000 |
| $\varepsilon_{su}^*$ | 0.075 | 0.075 |
| $\varepsilon_{tu}^*$ | 0.00184 | 0.01 |

*Assumed values

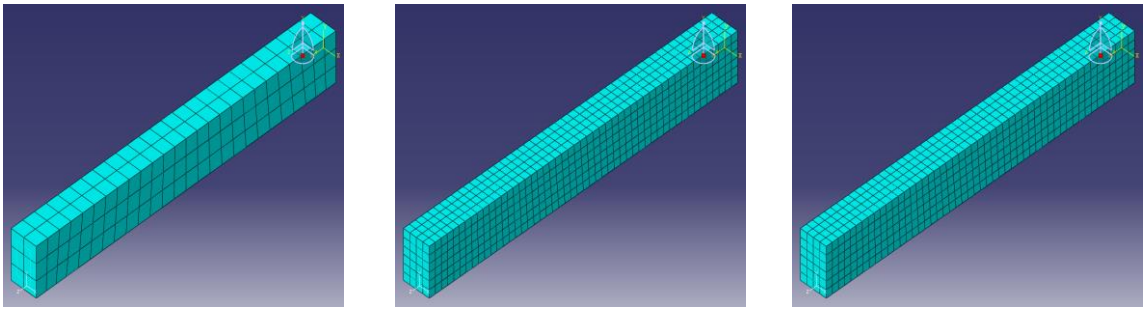

Fig. 9 Mesh configurations for beams

too. After approximately 1 hour, the plain concrete was prepared and poured on top of the ECC layer in order to prevent the mixing of ECC and concrete materials (Maalej and Li 1995). In this research, two beams (RC and Composite beams) are analyzed using ABAQUS program. To investigate the influence of mesh size on the results of the nonlinear analyses, three types of mesh configurations are used to analyze these beams. These mesh configurations including coarse, medium and fine mesh sizes, are shown in Fig. 9. Load-mid span deflection curves for the these two RC and composite beams are shown in Fig. 10 and Fig. 11, to investigate the influence of the size of elements. Cracking is idealized using the smeared cracking model, and is assumed to occur when the principal tensile stress at a point (usually a Gauss integration point) exceeds the tensile strength of the concrete. The stiffness across the crack is assumed to be zero and the principal directions are not allowed to rotate. For evaluation of an "appropriate" value of the ultimate tensile strain of the concrete, $\varepsilon_{tu}$, and elimination of mesh size dependency phenomenon, Shayanfar *et al*. proposed the following simple formula

$$\varepsilon_{tu} = 0.004 \cdot e^{-0.008 \cdot h} \tag{3}$$

where $h$ is the width of the element in mm. In concrete materials, finer mesh size does not always conclude to more exact response and there is a limit value for this case. Because, decreasing in

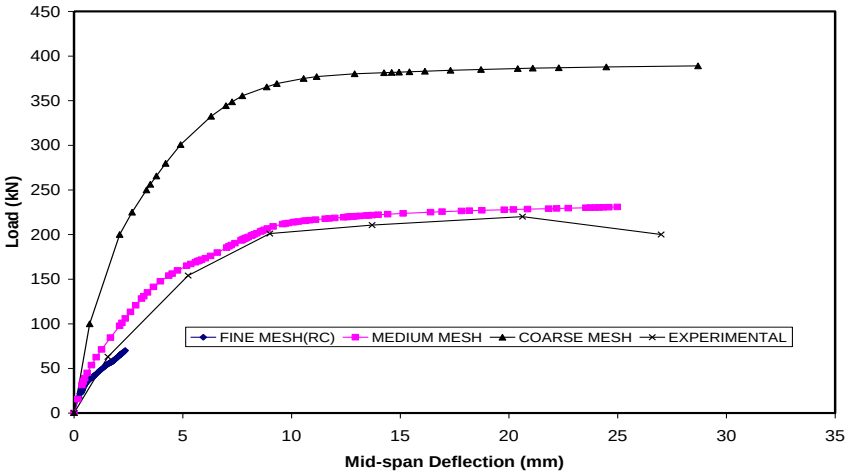


Fig. 10 Load-mid span deflection curves for different mesh sizes in RC beam

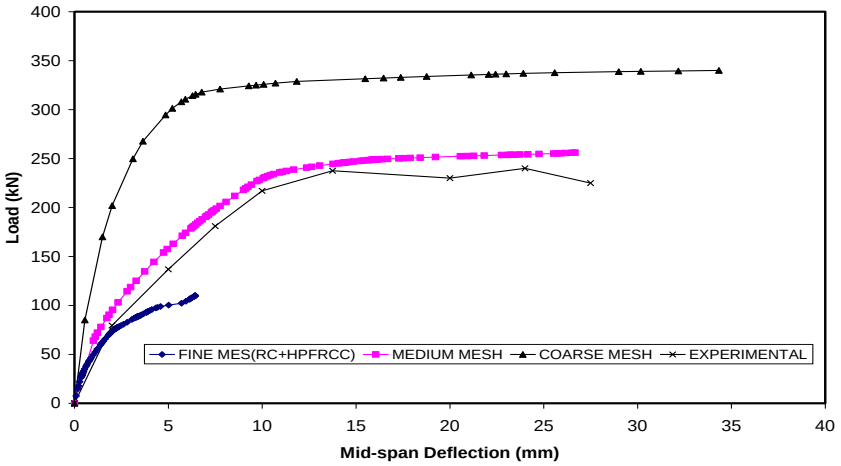


Fig. 11 Load-mid span deflection curves for different mesh sizes in composite beam

element size of concrete materials is concluded to more flexible beam and subsequently decreasing in ultimate force of the beam (Shayanfar *et al.* 1996).

In RC beams, the medium mesh size (50 mm×50 mm), gives an ultimate load value of 230.846 kN, which is close to the experimental value 208.2 kN. While the coarse mesh size (100 mm×100 mm), results in an ultimate load value 389.043 kN and the fine mesh size (25 mm×25 mm), concludes to an ultimate load 70 kN. Both of these values are very far from the experimental value. In composite beams, the medium mesh size gives an ultimate load value of 256 kN, which is close to the experimental value 234.7 kN. While the coarse mesh size results in an ultimate load value 340 kN and the fine mesh size concludes to an ultimate load 109.929 kN. Both of these values are very far from the experimental value. These analytical results are summarized in Table 3 and Table 4.

Table 3 Analytical and experimental results for RC beams with different mesh sizes

| Size of elements (mm×mm) | $P_u$ (Kn) | $\Delta_u$ (mm) | $\frac{P_u(Analytical)}{P_u(Experimental)}$ |
|---|---|---|---|
| 25 x 25 | 70 | 2.35004 | 0.34 |
| 50 x 50 | 230.846 | 24.9847 | 1.11 |
| 100 x 100 | 389.043 | 28.6998 | 1.86 |
| Experimental | 208.2 | 26.5 | - |

Table 4 Analytical and experimental results for composite beams with different mesh sizes

| Size of elements (mm×mm) | $P_u$ (Kn) | $\Delta_u$ (mm) | $\frac{P_u(Analytical)}{P_u(Experimental)}$ |
|---|---|---|---|
| 25×25 | 109.929 | 6.43779 | 0.47 |
| 50×50 | 256 | 26.6712 | 1.09 |
| 100×100 | 340 | 34.3325 | 1.45 |
| Experimental | 234.7 | 27.5 | - |

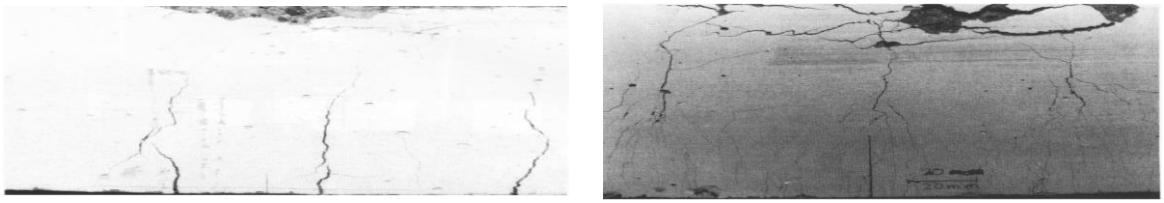

(a) RC beam (b) Composite beam

Fig. 12 Cracking patterns of beams in experimental work (Maalej *et al.* 2002)

As can be seen in Fig. 10 and Fig. 11, when a coarse mesh size is applied, the beam exhibits a stiffer behavior compared with the experimental response. With increasing the number of elements, the beam trends to be more flexible and less ductile. Infact, the mid span deflection at ultimate load decreases with reducing in element size. Hence, medium mesh size is selected for analytical purposes.

The cracking pattern of RC and composite beams in the experimental and analytical works are shown in Fig. 12 and Fig. 13 respectively. As shown in these figures, in RC beam, cracks occur at the bottom parts of the beam, i.e., in the tensile concrete. But in the composite beam, cracks first develop in the concrete part and then enter to the ECC layer, i.e., the main part of damage is occurred in the tensile concrete on top of the ECC layer which is shown by red color in bottom parts of Fig. 13(a) and (b). In experimental test, no sign of de-lamination between the ECC layer and concrete part was observed. These experimental findings are confirmed by analytical results. Some researchers have worked on size effect in flexural members and stated that ranging from small scale to structurally sized components, ECC members exhibit negligible size effect compared to reinforced concrete members. This size effect is more negligible for reinforced ECC members with longitudinal steel bars. This behavior is a result of the ductility of the ECC material (Lepech and Li 2003, Lepech and Li 2004, Kanakubo *et al.* 2007).

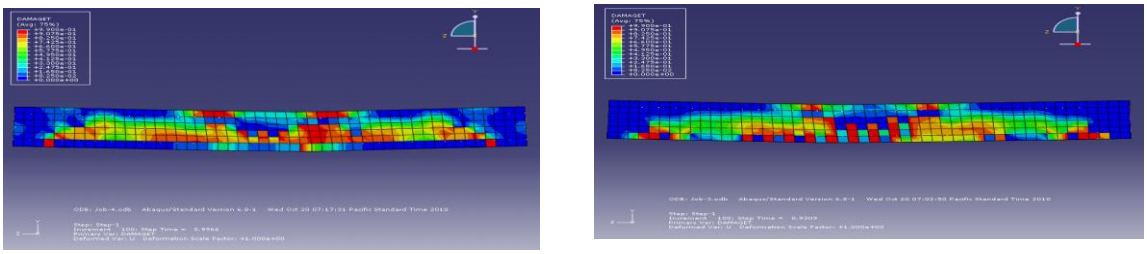

(a) RC beam (b) Composite beam

Fig. 13 Cracking pattern of beams in the analytical work

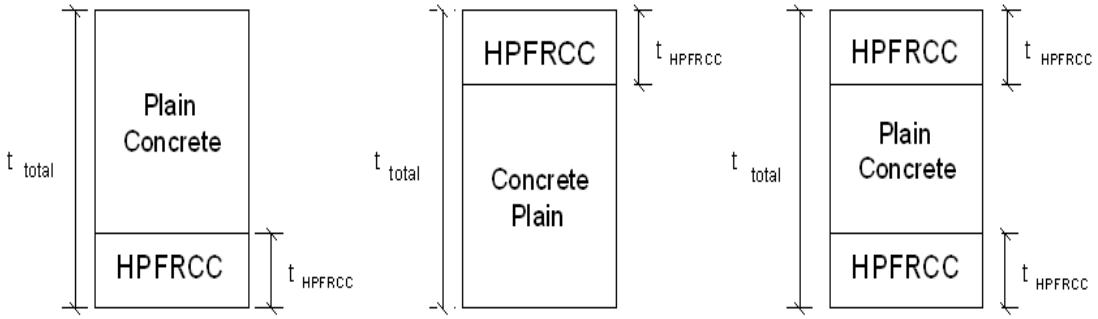


(a) (b) (c)

Fig. 14 Geometry of beams with different HPFRCC layers on top and in bottom

## 6. New composite specimens with different HPFRCC layer positions

In this paper, the experimental beams which have been tested by Maalej *et al.*, are selected and investigated. At first stage, the plain concrete that surrounds the tensile reinforcements, is replaced with HPFRCC material gradually, including $\frac{t_{HPFRCC}}{t_{total}} = 0.2 - 1$, according to Fig. 14. Then, the mechanical properties of these specimens are investigated with different thicknesses, different tensile strengths, different tensile strains of HPFRCC and different compressive bars. These stages are presented in Table 5.

## 7. Results

### *7.1 Effect of replaced HPFRCC layer in bottom of the beam*

Load-mid span deflection curves of RC and composite HPFRCC beams with different layer thicknesses in bottom of section (according to Fig. 14(a)) with ($\varepsilon_{tu}$=0.01) and ($f_t$=3 MPa) is shown in Fig. 15.

In RC beam, the first steel yielding appeared in the tensile reinforcements at a load of 190.323 kN and a mid span deflection of 7.40324 mm. As the load increased, the beam failed at the

Table 5 Analytical and experimental results for composite beams with different mesh sizes

| Name of Model | Position of HPFRCC Layer | $\frac{t_{HPFRCC}}{t_{total}}$ | $f_t$ (MPa) | $\varepsilon_{tu}$ | compression bars ($A_S'$) |
|---|---|---|---|---|---|
| B1 | Bot | 0.2 | 3 | 0.01 | 2 No. 13 |
| B2 | Bot | 0.4 | 3 | 0.01 | 2 No. 13 |
| B3 | Bot | 0.6 | 3 | 0.01 | 2 No. 13 |
| B4 | Bot | 0.8 | 3 | 0.01 | 2 No. 13 |
| B5 | Bot | 1 | 3 | 0.01 | 2 No. 13 |
| B6 | Top | 0.2 | 3 | 0.01 | 2 No. 13 |
| B7 | Bot+Top | 0.2+0.2 | 3 | 0.01 | 2 No. 13 |
| B8 | Bot | 0.2 | 3.5 | 0.01 | 2 No. 13 |
| B9 | Bot | 0.4 | 3.5 | 0.01 | 2 No. 13 |
| B10 | Bot | 1 | 3.5 | 0.01 | 2 No. 13 |
| B11 | Bot | 0.2 | 4 | 0.01 | 2 No. 13 |
| B12 | Bot | 0.4 | 4 | 0.01 | 2 No. 13 |
| B13 | Bot | 1 | 4 | 0.01 | 2 No. 13 |
| B14 | Bot | 0.2 | 3 | 0.015 | 2 No. 13 |
| B15 | Bot | 0.4 | 3 | 0.015 | 2 No. 13 |
| B16 | Bot | 1 | 3 | 0.015 | 2 No. 13 |
| B17 | Bot | 0.2 | 3 | 0.01 | 2 No. 16 |
| B18 | Bot | 0.4 | 3 | 0.01 | 2 No. 16 |
| B19 | Bot | 1 | 3 | 0.01 | 2 No. 16 |

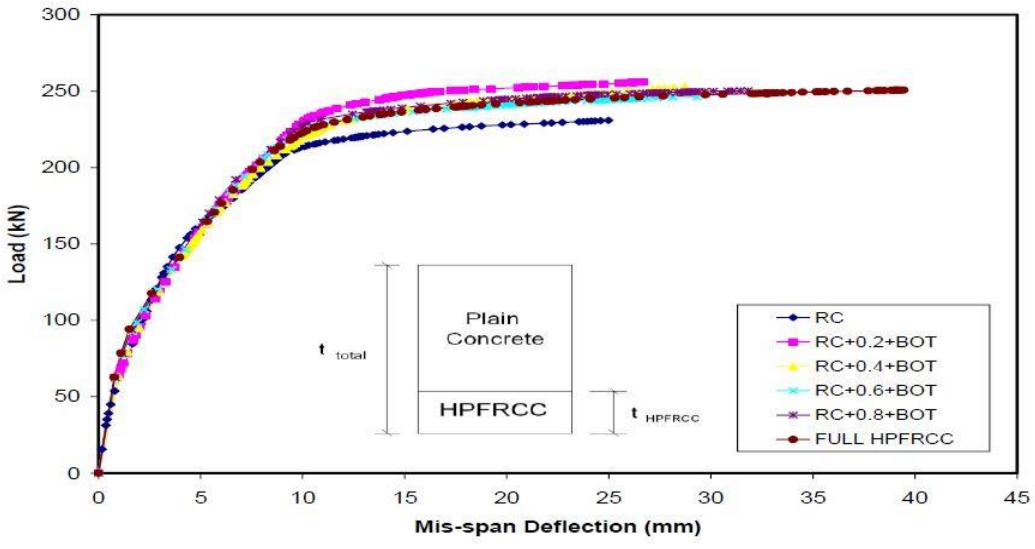


Fig. 15 Load-mid span deflection curve of RC, composite and full HPFRCC beams ($\varepsilon_{tu}$=0.01) and ($f_t$=3MPa)

ultimate load of 230.846 kN and mid span deflection of 24.9847 mm.

In composite beam B1 with $\frac{t_{HPFRCC}}{t_{total}} = 0.2$, the first cracks appeared in tensile concrete just above the HPFRCC layer. As the load increased, the first steel yielding appeared in the tensile reinforcements at a load of 211.218 kN and a mid span deflection of 8.55982 mm. As the load increased, the beam failed at the ultimate load of 256 kN and mid span deflection of 26.6712 mm. At this stage large tensile cracks occurred in the lower parts of the concrete part and the crushing of the compressive concrete progressed down to the beam. In this case, the most part of damages occurred in tension part too.

In composite beam B2 with $\frac{t_{HPFRCC}}{t_{total}} = 0.4$, the first cracks appeared in tensile concrete just above the HPFRCC layer. As the load increased, the first steel yielding appeared in the tensile and compressive steel reinforcements simultaneously at a load of 214.641 kN and a mid span deflection of 9.50632 mm. As the load increased, the beam failed at the ultimate load of 253 kN and mid span deflection of 28.7389 mm. In this case, the most part of damages occurred in tension part too and the amount of damage in HPFRCC and compressive part of the section seemed to be restricted.

In composite beam B3 with $\frac{t_{HPFRCC}}{t_{total}} = 0.6$, the first cracks appeared in HPFRCC material. As the load increased, the first steel yielding appeared in the compressive reinforcements at a load of 214.881 kN and a mid span deflection of 8.94392 mm. As the load increased, the beam failed at the ultimate load of 246.21 kN and mid span deflection of 29.3269 mm. In this case, the most part of damages occurred in compression part.

In composite beam B4 with $\frac{t_{HPFRCC}}{t_{total}} = 0.8$, the first cracks appeared in HPFRCC material. As the load increased, the first steel yielding appeared in the compressive reinforcements at a load of 216.96 kN and a mid span deflection of 8.90106 mm. As the load increased, the beam failed at the ultimate load of 250.4 kN and mid span deflection of 31.8303 mm. In this case, the most part of damages occurred in compression part.

In full HPFRCC beam B5 with $\frac{t_{HPFRCC}}{t_{total}} = 1$, the first cracks appeared in HPFRCC material. As the load increased, the first steel yielding appeared in the compressive reinforcements at a load of 217.934 kN and a mid span deflection of 9.39099 mm. As the load increased, the beam failed at the ultimate load of 250.625 kN and mid span deflection of 39.4389 mm. In this case, the most part of damages occurred in compression part. The yielding and ultimate loads, mid span deflections in yielding and ultimate loads and ductility ratios $\left(\mu = \frac{\Delta_u}{\Delta_y}\right)$ are summarized in Table 6.

Where: $P_{uRC}$ and $\Delta_{uRC}$ =Ultimate load and displacement values of RC beam.

As can be seen in this Fig. 15, the maximum ultimate load is attained by a composite beam with $\frac{t_{HPFRCC}}{t_{total}} = 0.2$. Increasing the $\frac{t_{HPFRCC}}{t_{total}}$ parameter, results in reducing the ultimate load value

Table 6 Analytical results for RC and composite beams with different layers of HPFRCC in bottom of the section

| Geometry of Beam | $P_y$ (kN) | $\Delta_y$ (mm) | $P_u$ (kN) | $\Delta_u$ (mm) | $\frac{P_u}{P_{uRC}}$ | $\frac{\Delta_u}{\Delta_{uRC}}$ | $\mu$ |
|---|---|---|---|---|---|---|---|
| RC | 190.323 | 7.40324 | 230.846 | 24.9847 | 1 | 1 | 3.3699 |
| (B1) Bot=0.2 | 211.218 | 8.55982 | 256 | 26.6712 | 1.109 | 1.0675 | 3.1158 |
| (B2) Bot=0.4 | 214.641 | 9.50632 | 253 | 28.7389 | 1.096 | 1.15 | 3.023 |
| (B3) Bot=0.6 | 214.881 | 8.94392 | 246.21 | 29.3269 | 1.066 | 1.174 | 3.279 |
| (B4) Bot=0.8 | 216.96 | 8.90106 | 250.4 | 31.8303 | 1.0847 | 1.274 | 3.576 |
| (B5)HPFRCC | 217.934 | 9.39099 | 250.625 | 39.4389 | 1.0856 | 1.578 | 4.199 |

compared to the beam with $\frac{t_{HPFRCC}}{t_{total}} = 0.2$. Because when a deep layer of HPFRCC material with high tensile strain in compared with regular concrete, is substituted in RC beam, the natural axis of the beam moves toward the bottom of the section and it results in higher strains in upper parts of the composite beam(compressive parts of the beam). This may be concluded to first yielding of compressive steel reinforcements and subsequently a decrease in ultimate load of the beam. Because, the compressive reinforcements of the beams are much less than their tensile reinforcements commonly. As it shown in Table 5, when the proportion of $\frac{t_{HPFRCC}}{t_{total}}$ reach to a value more than 0.8, the ultimate load of the beam increases again. Because with substituting of HPFRCC in the most parts of the RC beam, this composite beam converts to a section with a compression part which includes a material with higher compressive strength than normal concrete. Therefore, the beams with $\frac{t_{HPFRCC}}{t_{total}} = 0.8$ and 1, exhibits more ultimate loads. But with increase in $\frac{t_{HPFRCC}}{t_{total}}$ parameter of a composite beam, the ultimate mid span deflection of these beams increases. It can be achieved because of the high tensile capacity of the HPFRCC material compared with concrete. Hence, it should be noted that using HPFRCC material in lower parts of the composite sections, may be resulted in an increase in strength and mid span deflection capacity of the concrete beams. Szerszen *et al.* have been presented analytical closed-form solutions for reinforced HPFRCC moment-curvature responses which are shown in Eq. (4).

$$c = \frac{f_t \cdot h \cdot b + A_s \cdot f_y}{0.85 f_c' \times 0.66b + f_t \cdot b}$$
$$M = \frac{1}{2}\left[f_t \cdot (h-c)(h+c-a) \cdot b + A_s \cdot f_y \cdot (2d-a)\right] \quad (4)$$

Where, $c$=neutral axis depth and $a$=0.66c (equivalent rectangular stress block depth). If these equations applied for B5 model the ultimate moment and force are approximately equal to 80 kNm and 222 kN ($M = \frac{P}{2} \times 0.72$) respectively. This ultimate load is about 11% less than analytical model. This difference could be due to use of equivalent compressive stress block and elastic

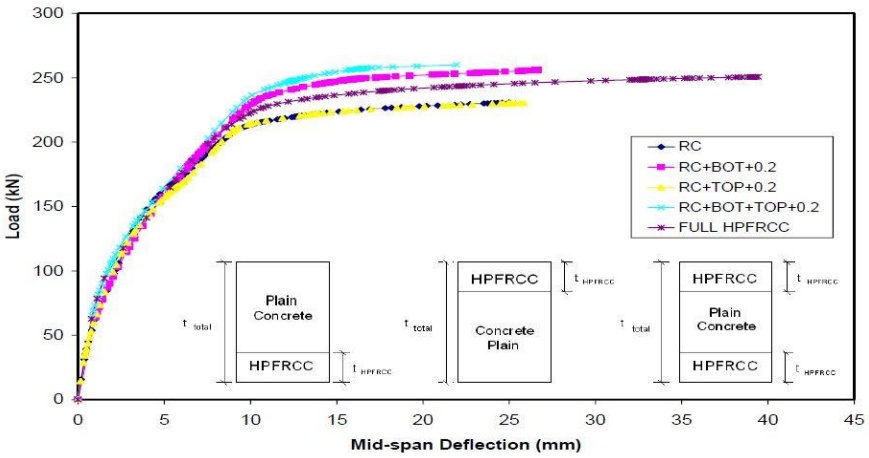


Fig. 16 Load-mid span deflection curve of RC and composite beams ($\varepsilon_{tu}$=0.01) and ($f_t$=3 MPa)

perfect plastic model for steel in this method (Szerszen *et al.* 2006, Hemmati *et al.* 2014).

### *7.2 Effect of replaced HPFRCC layer on top and bottom of the beam*

Load-mid span deflection curve of RC and composite beams with HPFRCC layers only on top and also on top plus bottom of the section(as shown in Fig. 14(b) and Fig. 14(c)) with ($\varepsilon_{tu}$=0.01) shown in Fig. 16.

In composite beam B6 with $\frac{t_{HPFRCC,TOP}}{t_{total}} = 0.2$, the first cracks appeared in tensile concrete. Behavior and mechanism of failure of this beam is very close to RC beam. Because, the compressive characteristics of HPFRCC and regular concrete have no significant differences. i.e., a small compression part of the beam is substituted with a material with high tensile characteristics and it could not be effective on the behavior of this flexural member.

In composite beam B7 with $\frac{t_{HPFRCC,TOP,BOT}}{t_{total}} = 0.2$, the first cracks appeared in tensile concrete just above the HPFRCC layer. Behavior and mechanism of failure of this beam is very close to composite beam with $\frac{t_{HPFRCC}}{t_{total}} = 0.2$. Compressive strength of HPFRCC in B7 model has been assumed to be same with compressive strength of concrete in RC beam. In this model authors want to show that compressive characteristics of the HPFRCC and regular concrete have no significant differences. The yielding and ultimate loads, mid span deflections in yielding and ultimate loads and ductility ratios $\left(\mu = \frac{\Delta_u}{\Delta_y}\right)$ of different beams with top and bottom HPFRCC layers are summarized in Table 7.

Table 7 Comparison of analytical results for composite beams with different position of HPFRCC layer

| Geometry of Beam | $P_y$ (Kn) | $\Delta_y$ (mm) | $P_u$ (Kn) | $\Delta_u$ (mm) | $\frac{P_u}{P_{uRC}}$ | $\frac{\Delta_u}{\Delta_{uRC}}$ | $\mu$ |
|---|---|---|---|---|---|---|---|
| (B6) Top=0.2 | 194.418 | 7.94131 | 231.4 | 25.8596 | 1.002 | 1.035 | 3.256 |
| (B7)Bot+Top=0.2 | 208.809 | 7.91927 | 259.937 | 21.9458 | 1.126 | 0.878 | 2.771 |

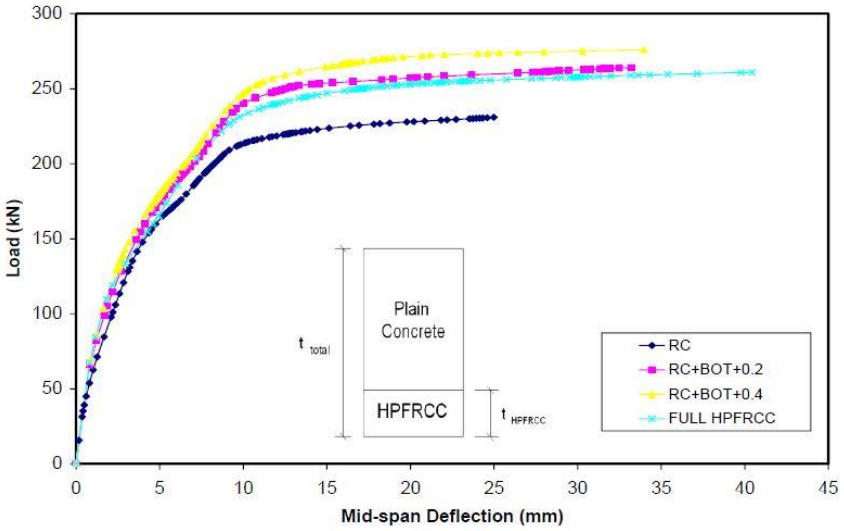


Fig. 17 Load-mid span deflection curve of RC and composite beams ($\varepsilon_{tu}$=0.01) and ($f_t$=3.5 MPa)

Table 8 Analytical results for composite and HPFRCC beams with $\varepsilon_{tu}$=0.01 and $f_t$=3.5 MPa

| Geometry of Beam | $P_y$ (Kn) | $\Delta_y$ (mm) | $P_u$ (kN) | $\Delta_u$ (mm) | $\mu$ | $\frac{P_u}{P_{uRC}}$ | $\frac{\Delta_u}{\Delta_{uRC}}$ |
|---|---|---|---|---|---|---|---|
| (B8) Bot=0.2 | 227.844 | 8.85564 | 264 | 33.207 | 3.749 | 1.143 | 1.329 |
| (B9) Bot=0.4 | 238.796 | 9.00014 | 275.997 | 33.9553 | 3.773 | 1.195 | 1.359 |
| (B10)HPFRCC | 226.022 | 9.12576 | 260.913 | 40.4452 | 4.4319 | 1.13 | 1.619 |

Hence, it should be noted that, in addition to improving the durability of the concrete beams, using HPFRCC material in upper parts of the composite sections, may not be effective compared with composite sections with bottom HPFRCC layers.

### *7.3 Effect of tensile strength of HPFRCC ($f_{t,HPFRCC}$)*

As could be seen in Fig. 15 and Table 5, the behavior of composite sections with $\frac{t_{HPFRCC}}{t_{total}} = 0.6$ and $\frac{t_{HPFRCC}}{t_{total}} = 0.8$ are very close to full HPFRCC beam. Therefore, in this part of paper, only two composite sections with $\frac{t_{HPFRCC}}{t_{total}} = 0.2$ (B8), $\frac{t_{HPFRCC}}{t_{total}} = 0.4$ (B9) and one full

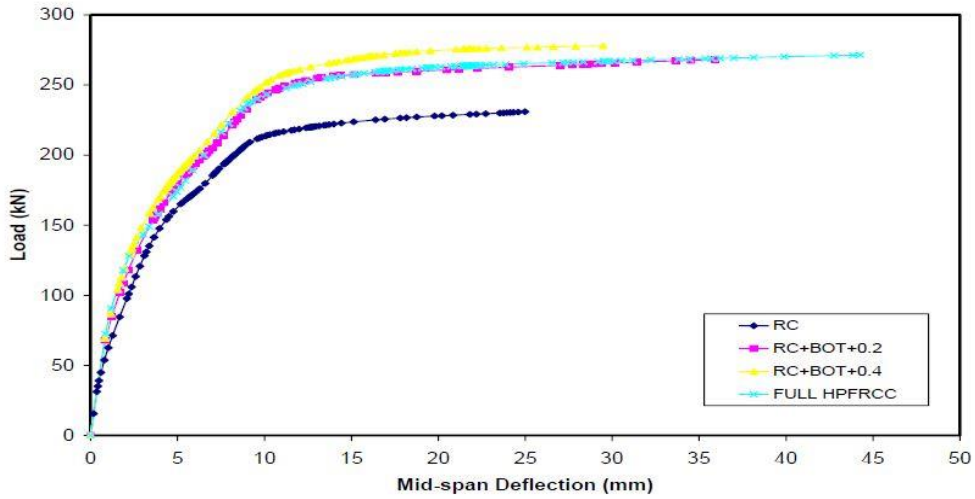


Fig. 18 Load-mid span deflection curve of RC and composite beams ($\varepsilon_{tu}$=0.01) and ($f_t$=4 MPa)

Table 9 Analytical results for composite and HPFRCC beams $\varepsilon_{tu}$=0.01 and $f_t$=4 MPa

| Geometry of Beam | $P_y$ (kN) | $\Delta_y$ (mm) | $P_u$ (kN) | $\Delta_u$ (mm) | $\mu$ | $\frac{P_u}{P_{uRC}}$ | $\frac{\Delta_u}{\Delta_{uRC}}$ |
|---|---|---|---|---|---|---|---|
| (B11) Bot=0.2 | 209.453 | 6.70639 | 268.063 | 35.9204 | 5.356 | 1.161 | 1.438 |
| (B12) Bot=0.4 | 241.851 | 9.0749 | 277.8 | 39.4824 | 4.3507 | 1.203 | 1.58 |
| (B13)HPFRCC | 222.452 | 7.94255 | 271.303 | 44.2664 | 5.573 | 1.175 | 1.771 |

HPFRCC beam (B10) are chosen in order to investigate the effect of $f_{t,HPFRCC}$ on behavior of composite section. Load-mid span deflection curves of RC, composite and full HPFRCC beams with $\varepsilon_{tu}$=0.01 and $f_{t,HPFRCC}$=3.5 MPa are shown in Fig. 17. Analytical results of these beams are presented in Table 8.

Analytical results show that, composite section with $\frac{t_{HPFRCC}}{t_{total}} = 0.4$ exhibits the maximum ultimate load value of 275.997 kN and full HPFRCC beam exhibits the ultimate mid span deflection with a value of 40.4452 mm.

Load-mid span deflection curves of RC, composite and full HPFRCC (B11, B12 and B13) beams with ($\varepsilon_{tu}$=0.01) and ($f_t$=4 MPa) are shown in Fig. 18. Analytical results of these beams are presented in Table 9.

Analytical results show that, composite section with $\frac{t_{HPFRCC}}{t_{total}} = 0.4$ exhibits the maximum ultimate load value of 277.8 kN and full HPFRCC beam exhibits the ultimate mid span deflection with a value of 44.2664 mm.

A comparison among full HPFRCC beams with $\varepsilon_{tu}$=0.01 and $f_t$=3,3.5 and 4 MPa is shown in Fig. 19 results show that, HPFRCC beam with $f_t$=4 MPa, has an ultimate load value about 4% and 8% more than HPFRCC with $f_t$=3.5 and 3 MPa respectively. Also, mid span deflection of

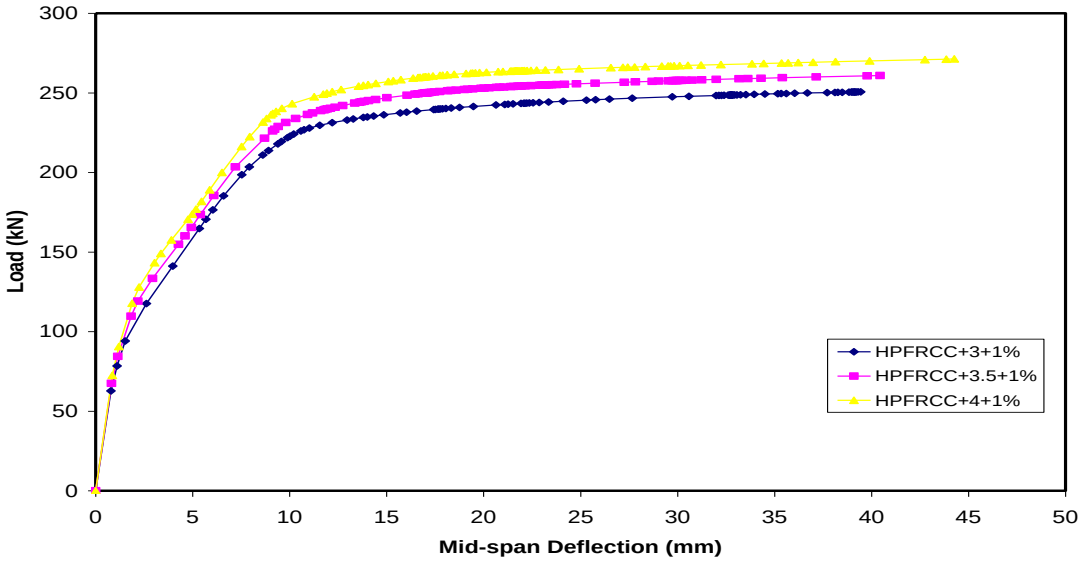


Fig. 19 Load-mid span deflection curve of HPFRCC beams ($\varepsilon_{tu}$=0.01) and ($f_t$=3,3.5 and 4 MPa)

Table 10 Effect of $f_{t,HPFRCC}$ on behavior of composite sections

| Geometry of Beam | $f_t$=3 MPa | | | | $f_t$=3.5 MPa | | | | $f_t$=4 MPa | | | |
|---|---|---|---|---|---|---|---|---|---|---|---|---|
| | $P_y$ (kN) | $\Delta_y$ (mm) | $P_u$ (kN) | $\Delta_u$ (mm) | $P_y$ (kN) | $\Delta_y$ (mm) | $P_u$ (kN) | $\Delta_u$ (mm) | $P_y$ (kN) | $\Delta_y$ (mm) | $P_u$ (kN) | $\Delta_u$ (mm) |
| RC | 190.32 | 37.4032 | 423 | 0.8462 | 4.9847 | 190.32 | 37.4032 | 423 | 0.8462 | 4.9847 | 190.32 | 37.4032 |
| Composite Bot=0.2 | 211.21 | 88.5598 | 256 | 26.6712 | 227.84 | 48.8556 | 264 | 33.207 | 209.45 | 36.7063 | 926 | 8.0633 |
| Composite Bot=0.4 | 214.64 | 19.5063 | 253 | 28.7389 | 238.79 | 69.0001 | 427 | 5.9973 | 353.95 | 241.851 | 9.0749 | 277.8 |
| Full HPFRCC | 217.93 | 49.3909 | 925 | 0.6253 | 9.4389 | 226.02 | 29.1257 | 626 | 0.9134 | 0.4452 | 222.45 | 27.9425 |

HPFRCC beam with $f_t$=4 MPa, increases about 9% and 12% compared to HPFRCC beams with $f_t$=3.5 and 3 MPa.

Hence, it may be concluded that, increasing in tensile strength of HPFRCC material ($f_t$), results in increase in ultimate load and mid span deflection of this beam. But, it seems that, the deflection of the beams is more influenced by this parameter. These analytical results are summarized in Table 10. Increasing the tensile strength of HPFRCC results in increased ultimate load and mid span deflection. But as it shown in Eq. (4) increasing in load is small. In this case the most part of increasing load is due to post yielding strength of steel reinforcements. Using HPFRCC material with higher tensile strength results in more unity under the loading and this unity concludes to achieve more deflections compare to loads. Moreover, increasing the tensile strength of HPFRCC results in increasing in neutral axis depth ($c$) and this phenomenon concludes to more compressive strain in HPFRCC and more tensile strain in steel and HPFRCC and subsequently, deflection of these beams increase more than their load.

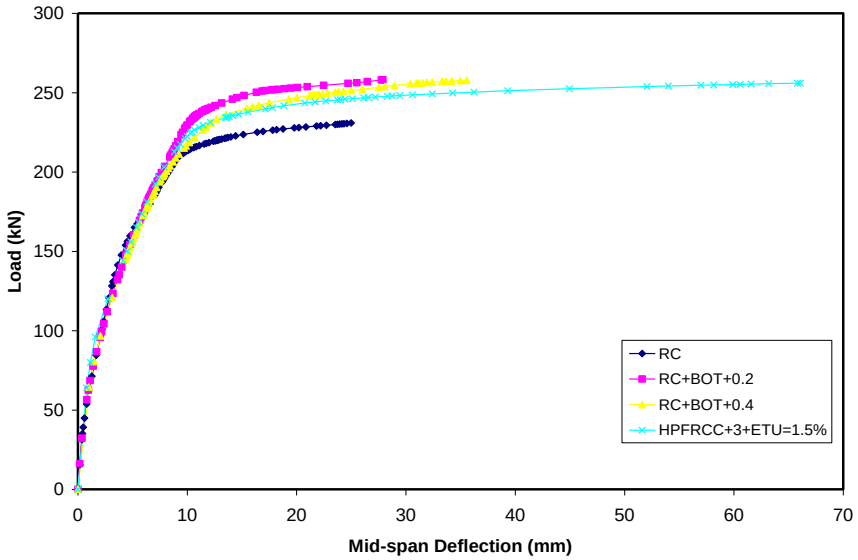


Fig. 20 Load-mid span deflection curve of RC and composite beams ($\varepsilon_{tu}$=0.015) and ($f_t$=3 MPa)

Table 11 Analytical results for RC, composite and HPFRCC beams with $\varepsilon_{tu}$=0.015 and $f_t$=3 MPa

| Geometry of Beam | $P_y$ (kN) | $\Delta_y$ (mm) | $P_u$ (kN) | $\Delta_u$ (mm) | $\mu$ | $\frac{P_u}{P_{uRC}}$ | $\frac{\Delta_u}{\Delta_{uRC}}$ |
|---|---|---|---|---|---|---|---|
| (B14) Bot=0.2 | 209.411 | 8.42176 | 258.1 | 27.8937 | 3.312 | 1.118 | 1.116 |
| (B15) Bot=0.4 | 211.356 | 9.247 | 257.8 | 35.5613 | 3.8457 | 1.116 | 1.423 |
| (B16)HPFRCC | 212.711 | 8.8286 | 256 | 66.0614 | 7.4826 | 1.109 | 2.644 |

### *7.4 Effect of ultimate compressive strain of HPFRCC ($\varepsilon_{tu}$)*

As could be seen in Fig. 15, the behavior of composite sections with $\frac{t_{HPFRCC}}{t_{total}} = 0.6$ and 0.8 are very close to full HPFRCC beam. Therefore, in this part of paper, composite sections with $\frac{t_{HPFRCC}}{t_{total}} = 0.2$ (B14), $\frac{t_{HPFRCC}}{t_{total}} = 0.4$ (B15) and full HPFRCC (B16) beams are considered to investigate the effect of ($\varepsilon_{tu}$). Load-mid span deflection curves of RC, composite and full HPFRCC beams with $\varepsilon_{tu}$=0.015 and $f_t$=3 MPa are shown in Fig. 20.

Analytical results of these beams with different values of ($\varepsilon_{tu}$) are presented in Table 11.

Analytical results show that, composite section with $\frac{t_{HPFRCC}}{t_{total}} = 0.2$ exhibits the maximum ultimate load value of 258.1 kN which is very close to composite section with $\frac{t_{HPFRCC}}{t_{total}} = 0.4$ and full HPFRCC beam exhibits the ultimate mid span deflection with a value of 66.0614 mm. A comparison between full HPFRCC beams with $f_t$=3 MPa and $\varepsilon_{tu}$=0.01 and 0.015 show that,

Table 12 Analytical results for beams with 2 No. 16 compression reinforcements

| Geometry of Beam | $P_y$ (kN) | $\Delta_y$ (mm) | $P_u$ (kN) | $\Delta_u$ (mm) | $\mu$ | $\frac{P_u}{P_{uRC}}$ | $\frac{\Delta_u}{\Delta_{uRC}}$ |
|---|---|---|---|---|---|---|---|
| (B17) Bot=0.6 | 219.010 | 8.87375 | 253.8 | 33.802 | 3.809 | 1.099 | 1.353 |
| (B18) Bot=0.8 | 223.718 | 9.2 | 255.88 | 37.2546 | 4.0494 | 1.108 | 1.491 |
| (B19) HPFRCC | 224.062 | 9.71729 | 256 | 46.1545 | 4.7497 | 1.109 | 1.847 |

HPFRCC beam with $\varepsilon_{tu}$=0.015, has an ultimate load value about 2% more than HPFRCC with $\varepsilon_{tu}$=0.01. Also, mid span deflection of HPFRCC beam with $\varepsilon_{tu}$=0.015, increases about 67% compared with HPFRCC beams with $\varepsilon_{tu}$=0.01.

Hence, it may be concluded that, increasing in tensile strain capacity of HPFRCC material ($\varepsilon_{tu}$), results in increase in ultimate load and mid span deflection of this beam. But, it seems that, the deflection of the beams is more influenced by this parameter. Moreover, the influence of this parameter on ultimate load capacity of the beam, could be neglected.

### *7.5. Effect of compressive reinforcement ($A'_S$)*

As mentioned before, in composite sections with $\frac{t_{HPFRCC}}{t_{total}} = 0.6$ and $\frac{t_{HPFRCC}}{t_{total}} = 0.8$ and full HPFRCC beams, the compressive steel reinforcements yield at first stage (before yielding of tensile rebars) and consequently, the ultimate load capacity could not be increased as the same as composite sections with $\frac{t_{HPFRCC}}{t_{total}} = 0.2$, $\frac{t_{HPFRCC}}{t_{total}} = 0.4$. Hence, it seems that, increasing the area of compressive steel reinforcements could be concluded to higher ultimate loads and mid span deflections. Therefore, in this part of the paper, 2 reinforcing rebars with diameter of 16 mm are substituted to existing rebars with diameter of 13 mm while $\varepsilon_{tu}$=0.01 and $f_t$=3 MPa. Results show that, using 2 No. 16 compressive rebars, result in increasing about 3% and 15% in ultimate load and deflection respectively compared to the same section with 2 No. 13. Moreover, using 2 No. 16 compressive rebars, result in increasing about 3.5% and 17% in ultimate load and deflection respectively compared to the same section with 2 No. 13. Analytical results for beams with 2 No. 16 as compressive reinforcements are shown in Table 12.

Results show that, using 2 No. 16 compressive rebars, result in increasing about 2% and 17% in ultimate load and deflection respectively compared to the same section with 2 No. 13. Hence, it seems that, for optimum using of HPFRCC in composite beams, the more compressive reinforcements may be needed to use in compressive part of the section. With changing in the diameter and number of these reinforcements, both tension and compression rebars could yield simultaneously. Also, the ductility of these beam increases too compared to corresponding sections with 2 No. 13 as compressive reinforcements. Moreover, with increasing the amount of compressive steel reinforcements, neutral axis depth of the section decreased and this concludes to more ductility ratio and subsequently more mid-span deflection.

A summary of all analytical results with different parameters is shown in Table 13.

Variation of ultimate load ($P_u$) versus the ($\frac{t_{HPFRCC}}{t_{total}}$) parameter, is shown in Fig. 21. As observed

Table 13 Summary of analytical results

| Parameters | | | $\frac{t_{HPFRCC}}{t_{total}}$ | | | | | Average |
|---|---|---|---|---|---|---|---|---|
| | | | 0.2 | 0.4 | 0.6 | 0.8 | 1 | |
| $f_{tHPFRCC}$ =VAR<br>$\varepsilon_{tu}$=1%<br>$A'_S$= 2 No. 13 | 3 MPa | $P_u$ (kN) | 256 | 253 | 246.21 | 250.4 | 250.625 | |
| | | $\Delta_u$ (mm) | 26.6712 | 28.7389 | 29.3269 | 31.8303 | 39.4389 | |
| | | $\mu$ | 3.1158 | 3.023 | 3.279 | 3.576 | 4.199 | |
| | 3.5 MPa | $P_u$ (kN) | 264 | 275.997 | - | - | 260.913 | |
| | | $\Delta_u$ (mm) | 33.207 | 33.9553 | - | - | 40.4452 | |
| | | $\mu$ | 3.749 | 3.773 | - | - | 4.4319 | |
| | | $\frac{(P_u)_{3.5}}{(P_u)_3}$ | 1.031 | 1.091 | - | - | 1.041 | 1.0543 |
| | | $\frac{(\Delta_u)_{3.5}}{(\Delta_u)_3}$ | 1.245 | 1.182 | - | - | 1.025 | 1.151 |
| | 4 MPa | $P_u$ (kN) | 268.063 | 277.8 | - | - | 271.303 | |
| | | $\Delta_u$ (mm) | 35.9204 | 39.4824 | - | - | 44.2664 | |
| | | $\mu$ | 5.356 | 4.3507 | - | - | 5.573 | |
| | | $\frac{(P_u)_4}{(P_u)_3}$ | 1.047 | 1.098 | - | - | 1.082 | 1.076 |
| | | $\frac{(\Delta_u)_4}{(\Delta_u)_3}$ | 1.347 | 1.374 | - | - | 1.122 | 1.281 |
| $\varepsilon_{tu}$=*VAR*<br>$f_{tHPFRCC}$ = 3 MPa<br>$A'_S$= 2 No. 13 | 1 % | $P_u$ (kN) | 256 | 253 | 246.21 | 250.4 | 250.625 | |
| | | $\Delta_u$ (mm) | 26.6712 | 28.7389 | 29.3269 | 31.8303 | 39.4389 | |
| | | $\mu$ | 3.1158 | 3.023 | 3.279 | 3.576 | 4.199 | |
| | 1.5 % | $P_u$ (kN) | 258.1 | 257.8 | - | - | 256 | |
| | | $\Delta_u$ (mm) | 27.8937 | 35.5613 | - | - | 66.0614 | |
| | | $\mu$ | 3.312 | 3.8457 | - | - | 7.4826 | |
| | | $\frac{(P_u)_{1.5\%}}{(P_u)_{1\%}}$ | 1.008 | 1.019 | - | - | 1.021 | 1.016 |
| | | $\frac{(\Delta_u)_{1.5\%}}{(\Delta_u)_{1\%}}$ | 1.046 | 1.237 | - | - | 1.675 | 1.319 |
| $A'_S$=*VAR*<br>$\varepsilon_{tu}$=1%<br>$f_{tHPFRCC}$ = 3 MPa | 2 No. 13 | $P_u$ (kN) | 256 | 253 | 246.21 | 250.4 | 250.625 | |
| | | $\Delta_u$ (mm) | 26.6712 | 28.7389 | 29.3269 | 31.8303 | 39.4389 | |
| | | $\mu$ | 3.1158 | 3.023 | 3.279 | 3.576 | 4.199 | |
| | 2 No. 16 | $P_u$ (kN) | - | - | 253.8 | 255.88 | 256 | |
| | | $\Delta_u$ (mm) | - | - | 33.802 | 37.2546 | 46.1545 | |
| | | $\mu$ | - | - | 3.809 | 4.0494 | 4.7497 | |
| | | $\frac{(P_u)_{16}}{(P_u)_{13}}$ | - | - | 1.031 | 1.022 | 1.021 | 1.025 |
| | | $\frac{(\Delta_u)_{16}}{(\Delta_u)_{13}}$ | - | - | 1.152 | 1.17 | 1.17 | 1.164 |

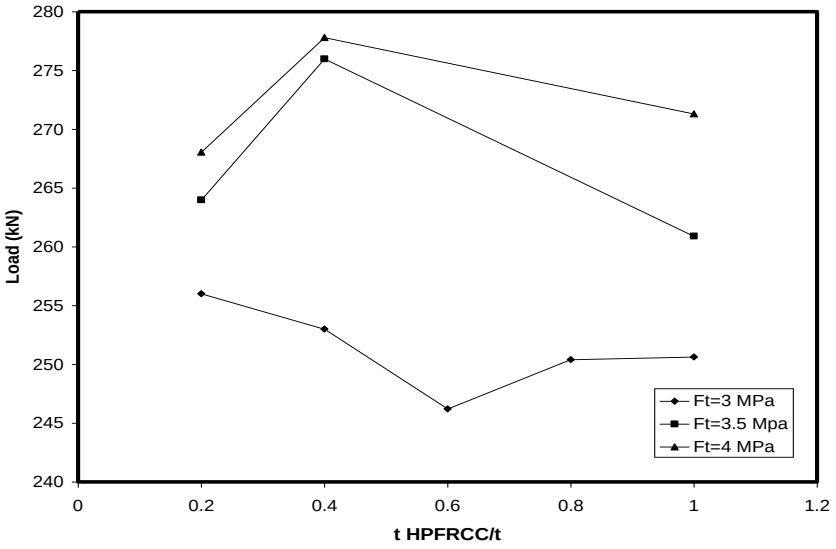


Fig. 21 Variation of ultimate load ($P_u$) versus the ($\frac{t_{HPFRCC}}{t_{total}}$) parameter

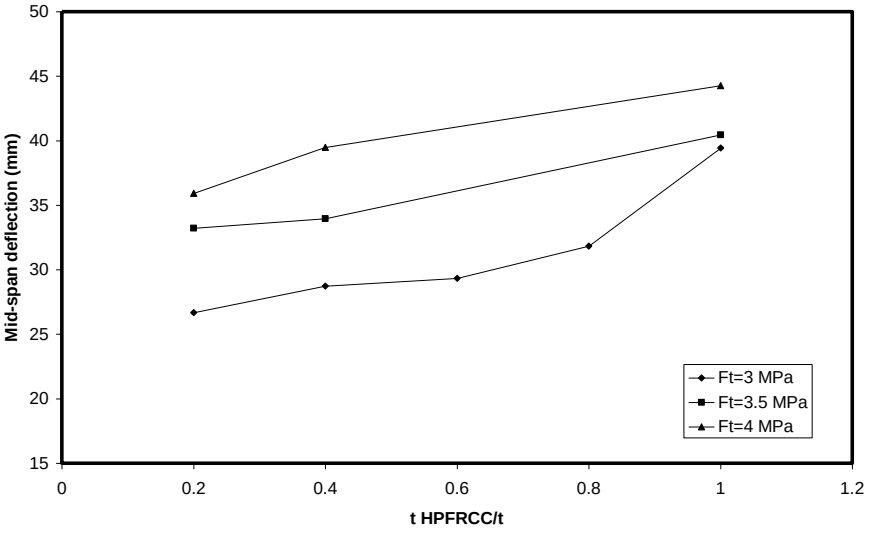


Fig. 22 Relation of mid-span deflection ($\Delta_u$) and the ($\frac{t_{HPFRCC}}{t_{total}}$) parameter

in this figure, the best option for $P_u$ is occurred at $\frac{t_{HPFRCC}}{t_{total}}$=0.2 to 0.4. Variation of ultimate mid-span deflection ($\Delta_u$) versus the ($\frac{t_{HPFRCC}}{t_{total}}$) parameter, is shown in Fig. 22. As observed in this

figure, the best option for $\Delta_u$ is occurred at $\frac{t_{HPFRCC}}{t_{total}}$ =1.

## 8. Conclusions

HPFRCC is a relatively new high performance material. Mechanical properties of HPFRCC depend on a large number of fiber and matrix parameters such as fiber length, fiber diameter, fiber aspect ratio, fiber-matrix interaction, matrix fracture toughness, matrix first cracking stress, etc. HPFRCC can be used in critical parts of a reinforced concrete beams and frames which are exposed to cracking in order to increase the capacity and durability of the structures. When a layer of HPFRCC is substituted to regular concrete in a RC beam, the durability of this beam improved.

Using this layer of HPFRCC in bottom of the beam section is more effective than using it on top of the section. This layer of HPFRCC concludes to attaining higher ultimate load and mid span deflection values compared to a RC beam. Increasing in tensile strength of HPFRCC material ($f_t$), results in increase in ultimate load and mid span deflection of the beam. But, it seems that, the deflection of these beams is more influenced by this parameter. Increasing in tensile strain capacity of HPFRCC material ($\varepsilon_{tu}$), results in little increase in ultimate load and more increase in mid span deflection of the beam. But, it seems that, the deflection of the beams is more influenced by this parameter. Moreover, the influence of this parameter on ultimate load capacity of the beam could be neglected. Also, increasing the area of compressive steel reinforcements could be concluded to higher ultimate load and mid span deflection. In these beams, the best options for $P_u$ and $\Delta_u$ are occurred at $\frac{t_{HPFRCC}}{t_{total}}$ =0.2 to 0.4 and $\frac{t_{HPFRCC}}{t_{total}}$ =1 respectively.

## References

Brandt, A.M. (2008), "Fiber reinforced cement-based (FRC) after over 40 years of development in building and civil engineering", *Compos. Struct.*, **86**, 3-9.

Chao, C.G., Ha, G.J. and Kim, Y.Y. (2008), "Nonlinear model of reinforced concrete frames retrofitted by in-filled hpfrcc walls", *Struct. Eng. Mech.*, **30**(2), 211-223.

Fischer, G., and Li, V. C. (2000), "Structural composites with ECC", *Proceeding of the ASCCS-6, International Conference on Steel-Concrete Composite Structures*, Los Angeles.

Fischer, G., Wang, S. and Li, V.C. (2003), "Design of engineered cementitious composites for processing and workability requirements", *Seventh International Symposium on Brittle Matrix Composites*, Warsaw, Poland.

Fukuyama, H., Matsuzaki, Y., Sato, Y. and Iso, M. (2000), "Structural performance of engineered cementitious composite elements".

Gencturk, B. and Elnashai, A.S. (2013), "Numerical modeling and analysis of ECC structures", *Mater. Struct.*, **46**(4), 663-682.

Ghobarah, A. and Aly, N.M. (1998), "Seismic reliability assessment of existing reinforced concrete buildings", *J. Earthq. Eng.*, **2**(4), 569-592.

Han, T.S., Feenstra, P.H. and Billington, S.L. (2003), "Simulation of highly ductile fiber-reinforced cement-based composite components under cyclic loading", *ACI Struct. J.*, **100**(6), 749-757.

Hemmati, A., Kheyroddin, A. and Sharbatdar, M.K. (2014), "Plastic hinge rotation capacity of reinforced HPFRCC beams", *J. Struct. Eng.*, **141**(2), 04014111.

Hemmati, A., Kheyroddin, A. and Sharbatdar, M.K. (2014), "Proposed equations for estimating the flexural characteristics of reinforced HPFRCC beams", *IJST, Tran. Civil Eng.*, **38**(C2), 395-407.
Kabele, P. and Horii, H. (1996), "Analytical model for fracture behaviors of pseudo strain-hardening cementitious composites", *J. Mater. Concrete Struct. Pavem.*, **30**(532), 208-219.
Hung, C.C. and El-Tawil, S. (2010), "Hybrid rotating/fixed-crack model for high performance fiber reinforced cementitious composites", *ACI Mater. J.*, **107**(6), 568-576.
Help of ABAQUS (2008), *Getting Started with ABAQUS*.
Kabele, P. (2000), "Assessment of structural performance of engineered cementitious composites by computer simulation", Habilitation Thesis, Csech Technical University in Prague.
Kanakubo, T., Shimizu, K. and Kanda, T. (2007), "Size effect on flexural and shear behavior of PVA-ECC", *Structures under Extreme Loading*.
Kong, H.J., Bike, S. and Li, V.C. (2003), "Development of a self-compacting engineered cementitious composite employing electrosteric dispersion/stabilization", *J. Cement Concrete Compos.*, **25**(3), 301-309.
Lee, B.Y., Kim, J.K. and Kim, Y.Y. (2010), "Prediction of ECC tensile stress-strain curves based on modified fiber bridging relations considering fiber distribution characteristics", *Comput. Concrete*, **7**(5), 455-468.
Lepech, M.D. and Li, V.C. (2003), "Preliminary findings on size effect in ECC structural members in flexure", *Brittle Matrix Composite-7*, Poland.
Lepech, M.D. and Li, V.C. (2004), "Size effect in ECC structural members in flexure", *Fract. Mech. Concrete Struct.*, 1059-1066.
Lepech, M.D., Li, V.C., Robertson, R.E. and Keoleian, G.A. (2007), "Design of ductile engineered cementitious composites for improved sustainability", *ACI Mater. J.*, **105**(6), 567-575.
Li, V.C. and Wu, H.C. (1992), "Conditions for pseudo strain-hardening in fiber reinforced brittle matrix composites", *J. Appl. Mech. Rev.*, **45**(8), 390-398.
Li, V.C. (2007), "Engineered cementitious composites (ECC)-material, structural, and durability performance", University of Michigan, Ann Arbor, MI 48109.
Maalej, M. and Li, V.C. (1995), "Introduction of strain hardening engineered cementitious composites in design of reinforced concrete flexural members for improved durability", *ACI Struct. J.*, **92**(2), 167-176.
Maalej, M., Ahmed, S.F.U. and Paramasivam, P. (2002), "Corrosion durability and structural response of functionally-graded concrete beams", *JCI International workshop on ductile fiber reinforced Cementitious composites (DFRCC)-Application and Evaluation*, Japan.
Mortezaej, A.R., Kheyroddin, A. and Ronagh, H.R. (2010), "Finite element analysis and seismic rehabilitation of a 1000-year-old heritage listed tall masonry mosque", *Struct. Des. Tall Spec. Build.*, 161-170.
Na, C. and Kwak, H.G. (2011), "A numerical tension stiffening model for ultra high strength fiber reinforced concrete beams", *Comput. Concrete*, **8**(1), 1-22.
Naaman, A.E. and Reinhardt, H.W. (1996), "Characterization of high performance fiber reinforced cement composites", *HPFRCC2*, England.
Parsekian, G.A., Shrive, N.G., Brown, T.G., Kroman, J., Seibert, P.J., Perry, V.H. and Boucher, A. (2008), *Innovative Ultra High Performance Concrete Structures*, Tailor made concrete structures, CRC Press.
Ranzi, G. and Bradford, M.A. (2009), "Nonlinear analysis of composite beams with partial shear interaction by means of the direct stiffness method", *Steel Compos. Struct.*, **9**(2), 131-158.
Shaheen, E. and Shrive, N.G. (2008), "Cyclic loading and fracture mechanics of Ductal concrete", *Int. J. Fract.*, **148**(3), 251-260.
Shai, G. and Mo, Y.L. (2008), *High Performance Construction Materials, Science and Applications*, World Scientific Publishing Co.
Shayanfar, M.A., Kheyroddin, A. and Mirza, M.S. (1996), *Element Size Effects in Nonlinear Analysis of Reinforced Concrete Members*, Computers & Structures, London, U.K.
Sirijaroonchai, K. (2009), "A macro-scale plasticity model for high performance fiber reinforced cement composites", PhD Dissertation, Michigan University.

Suwannakarn, S.W. (2009), "Post-cracking characteristics of high performance fiber reinforced cementitious composites", PhD Dissertation, Michigan University.
Szerszen, M.M., Szwed, A. and Li, V.C. (2006), "Flexural response of reinforced beam with high ductility concrete material", *Proc. Int. Symp. "Brittle Matrix Composites 8*, Warsaw.
Wang, S. and Li, V.C. (2003), "Materials design of lightweight PVA-ECC", *In Proc., HPFRCC*.
Wang, S. and Li, V.C. (2006), "High early strength engineered cementitious composites", *ACI Mater. J.*, **103**(2), 97-105.
Zhu, G., Yang, Y., Xue, J. and Nie, J. (2013), "Experimental and theoretical research on mechanical behavior of innovative composite beams", *Steel Compos. Struct.*, **14**(4), 313-333.

*CC*